GA-A--20276

DE91 005396

GA-A20276

COMPARISON BETWEEN THE ELECTRON CYCLOTRON CURRENT DRIVE EXPERIMENTS ON DIII-D AND PREDICTIONS FOR T-10

by

JOHN LOHR, R.A. JAMES,* G. GIRUZZI,† Y. GORELOV,‡
J. DeHAAS,§ R.W. HARVEY, T.C. LUCE, KYOKO MATSUDA,
C.P. MOELLER, C.C. PETTY, and R. PRATER

This is a preprint of a paper to be presented at the International Workshop Strong Microwaves in Plasma, September 18–23, 1990, in Suzdal, U.S.S.R. and to be printed in the *Proceedings*.

Work supported by
U.S. Department of Energy
Contract Nos. DE-AC03-89ER51114
and W-7405-ENG-48

* Lawrence Livermore National Laboratory.
† Association Euratom-CEA, Tore Supra Cadarache, France.
‡ Kurchatov Institute for Atomic Energy, Moscow.
§ Joint European Torus.

GENERAL ATOMICS PROJECT 3466
NOVEMBER 1990

GENERAL ATOMICS

MASTER

COMPARISON BETWEEN THE ELECTRON CYCLOTRON CURRENT DRIVE EXPERIMENTS ON DIII–D AND PREDICTIONS FOR T–10*

John Lohr, R.A. James,† G. Giruzzi,‡ Y. Gorelov,¶ J. DeHaas,§
R.W. Harvey, T.C. Luce, Kyoko Matsuda, C.P. Moeller, C.C. Petty, and R. Prater
General Atomics, P.O. Box 85608, San Diego, California 92186-9784, USA

ABSTRACT

Electron cyclotron current drive has been demonstrated on the DIII–D tokamak in an experiment in which ~1 MW of microwave power generated ~50 kA of non-inductive current. The rf-generated portion was about 15% of the total current. On the T-10 tokamak, more than 3 MW of microwave power will be available for current generation, providing the possibility that all the plasma current could be maintained by this method.

Fokker-Planck calculations using the code CQL3D and ray tracing calculations using TORAY have been performed to model both experiments. For DIII–D the agreement between the calculations and measurements is good, producing confidence in the validity of the computational models. The same calculations using the T-10 geometry predict that for $n_e(0) \sim 1.8 \times 10^{13}$ cm^{-3}, and $T_e(0) \sim 7$ keV, 1.2 MW, that is, the power available from only three gyrotrons, could generate as much as 150 kA of non-inductive current. Parameter space scans in which temperature, density and resonance location were varied have been performed to indicate the current drive expected under different experimental conditions.

The residual dc electric field was considered in the DIII–D analysis because of its nonlinear effect on the electron distribution, which complicates the interpretation of the results.

*Work supported by the U.S. Department of Energy under Contract Nos. DE-AC03-89ER51114 and W-7405-ENG-48.
†Lawrence Livermore National Laboratory.
‡Association Euratom-CEA, Tore Supra Cadarache, France.
¶Kurchatov Institute for Atomic Energy, Moscow.
§Joint European Torus.

A 110 GHz ECH system is being installed on DIII–D. Initial operations, planned for late 1991, will use four gyrotrons with 500 kW each and 10 second output pulses. Injection will be from the low field side from launchers which can be steered to heat at the desired location. These launchers, two of which are presently installed, are set at 20 degrees to the radial and rf current drive studies are planned for the initial operation.

I. INTRODUCTION

Within the past few years encouraging progress has been made in tokamak fusion research which has indicated that the path to a successful demonstration experiment, though rocky perhaps, is at least clear of major obstacles. This optimistic forecast has heightened interest in experiments relevant to a tokamak fusion reactor operating continuously, such as non-inductive current generation.

One candidate for non-inductive current drive is the asymmetric interaction in velocity space between the plasma electrons and injected electromagnetic waves at the electron cyclotron resonance frequencies. First demonstrated on the CLEO tokamak [1], EC current drive is the subject of ambitious programs on both the DIII–D and T–10 devices.

Although the theory of electron cyclotron damping is well understood, details of the experiments, such as localized pumpout of portions of the velocity distribution, interaction with relativistically downshifted resonances, refraction and so on leave considerable room for creative prognostication and interpretation of the results. In this paper we discuss the application of two fundamental analysis tools, Fokker-Planck calculations and ray tracing, to the experiments on these two tokamaks both to understand previous experiments and thereby benchmark the analysis and to predict the results of work planned for the near future.

II. THE ELECTRON CYCLOTRON CURRENT DRIVE INSTALLATIONS

A. DIII–D

The DIII–D ECH installation consists of ten gyrotrons each of which generates approximately 200 kW at 60 GHz in pulses 0.5 sec in duration. The transmission lines propagate the TE_{01} mode with approximately 85% efficiency. The waves were launched in the X–mode fundamental from the high field side of the tokamak at an angle of 17 degrees to the radial. The technical details of the installation have been described previously [2].

B. T–10

On T–10, 11 gyrotrons, each producing up to 400 kW in pulses up to one second long will be available. Nine of the tubes operate at 81 GHz and inject with a tangential component so that the microwaves cross the magnetic axis at an angle of 30 degrees to the radial. Two tubes are at 75 GHz with radial injection for heating only. A schematic of the installation and representative TORAY output indicating the model geometry for the midplane launcher is shown in Fig. 1. The power is launched in the O–mode at the fundamental from four toroidal locations, each of which has a slightly different geometry. For simplicity, these modelling calculations all use the "sector B" arrangement, which has three beamlines at 81 GHz, one of which is at the midplane with two others arranged symmetrically above and below it. The three lines are aimed so that the launched waves intersect at the geometric center of the tokamak.

III. THE ANALYSIS CODES

A. Ray Tracing

The General Atomics version of the code TORAY [3] was used for all the ray tracing studies reported here. The dispersion relation is calculated for the superposition of a relativistic Maxwellian distribution function and a superthermal tail characterized by forward, backward, and perpendicular temperatures

$$f = \underbrace{n_e(1-\alpha)\, f_0(T_e)}_{\text{Maxwellian}} + \underbrace{\alpha\, n_e\, f_1(T_{\parallel f}, T_{\parallel b}, T_\perp)}_{\text{tail}} \quad . \tag{1}$$

All quantities are functions of ρ, the normalized flux coordinate. Damping of an electromagnetic wave is calculated from the dispersion relation and the driven current is estimated from Cohen's theory [4].

TORAY is interfaced to General Atomics' transport code ONETWO [5] so that kinetic and Z_{eff} profiles can be input directly to a self-consistent calculation of the loop voltage.

For the T–10 calculations, a half power half width of 3 degrees was used and 18 rays were followed for each launcher from a point at the approximate location of the ceramic vacuum window. The plane mirror was not included in the model. The DIII–D calculations used 30 rays and a half power half width of about 7 degrees.

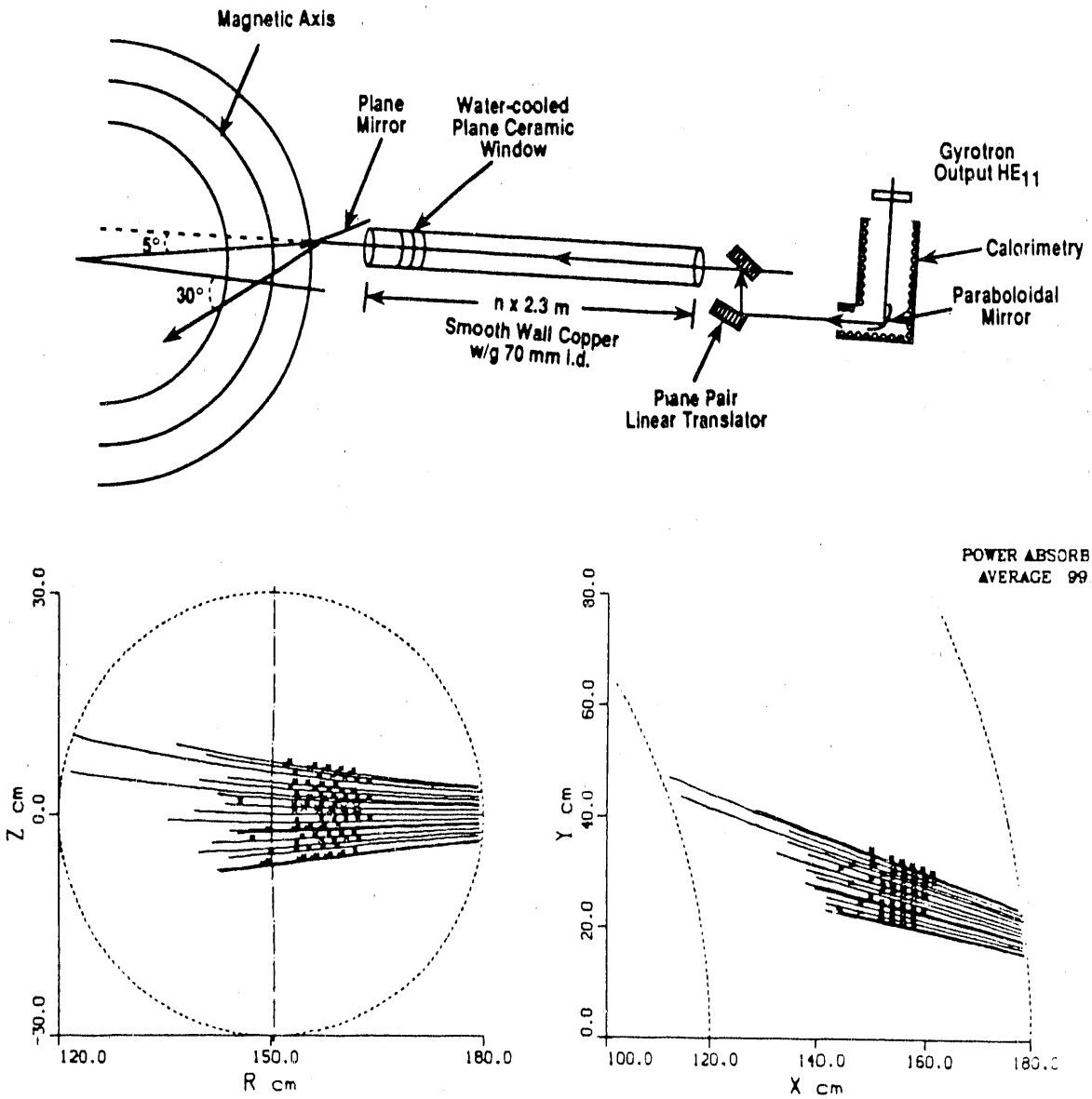

Fig. 1. Schematic representation of the waveguide installation on T–10. Also shown is a typical TORAY plot of the launch geometry and power deposition for the ECH resonance at the geometric center of the machine. For clarity, only the midplane bundle is shown. Parameters were $T_e(0) = 5$ keV, $n_e(0) = 3 \times 10^{13}$ cm^{-3}, $B_T(0) = 2.89$ T.

B. Fokker Planck

The Fokker-Planck calculations were done either with the code CQL3D [6], which calculates the two-dimensional bounce-averaged relativistic electron velocity distribution function at each point in a radial array or with the code of Giruzzi [7]. The ECH energy deposition model in CQL3D includes quasi-linear damping along a single ray but models the spread of the beam by a spectrum in $k_{||}$. This model is sharper in k-space than the actual experiment.

The code solves

$$\frac{\partial f_0}{\partial t}\ (\bar{v}_{\parallel 0}, v_{\perp 0}, r, t) = C(f_0) + Q(f_0) \quad ,$$

at each radial location and the rf energy transport equation

$$\nabla \cdot (v_g\, \epsilon) = -P_{\rm ABS}(r, \theta_{\rm pol}) = -\int d\bar{v}\ 2\, m v^2 Q(f) \quad ,$$

where C and Q are the collisional and quasi-linear operators respectively, f_0 is the midplane electron distribution function, ϵ is the rf energy density and v_g is the group velocity.

IV. RESULTS

The two codes described above have been used to model the electron cyclotron current drive experiments on DIII–D and T–10. For DIII–D, calculations for high field launch X–mode fundamental current drive are compared with the experimental data. Predictions for low field X–mode second harmonic and low field O–mode fundamental current drive on DIII–D have also been made. For T–10, the expected fundamental low field O–mode current drive was calculated. Variation of the parameters indicates the sensitivity to launch angle, resonance location, density and temperature.

A. DIII–D High Field X–Mode Fundamental Current Drive

TORAY, CQL3D, and Giruzzi's Fokker-Planck code have been applied to the analysis of the electron cyclotron current drive experiment on DIII–D. Using 30 rays to represent the Gaussian beam, TORAY predicted current drive efficiencies of 0.04 $\rightarrow$ 0.12 amperes/watt. The TORAY predictions assuming zero residual dc electric field in the plasma (i.e., full current drive) are plotted in Fig. 2 for a representative equilibrium and different scaled temperatures and densities. For these discharges the inductive electric field was not decreased to zero during the rf pulse and this complicates the analysis.

Electrons heated or accelerated by the rf move into the tail of the distribution function where they are less collisional. If subjected to an accelerating dc electric field, they then move to still higher energies under the influence of the field. This apparently rf-induced current is not strictly speaking "rf-driven" because should the inductive electric field decrease to zero this portion of the driven current, for fields well below the critical runaway field, also disappears.

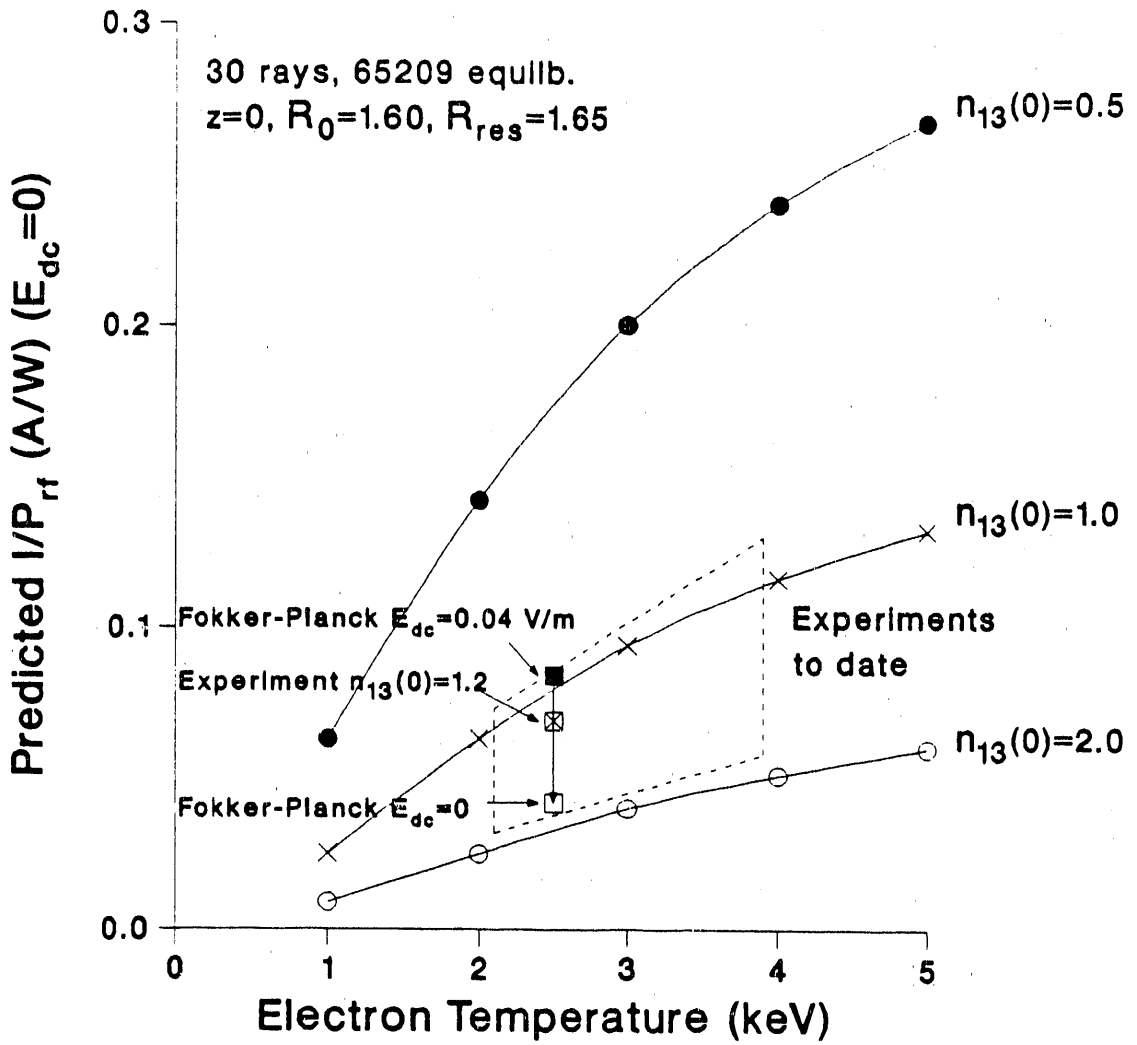

Fig. 2. TORAY calculations of rf current drive for the DIII–D high field launch X–mode fundamental experiment. The predicted 50 kA non-inductive current is in reasonable agreement with the measurements.

An estimate of the importance of this "inductively driven, rf augmented" current is indicated by three points in Fig. 2. The upper point is the current predicted by Fokker Planck calculation assuming $E_{\rm dc} = 0.04$ V/m, the experimentally measured value. The middle point is the total current inferred from the measured kinetic profiles and the measured $Z_{\rm eff}$ profile assuming neoclassical resistivity. Finally, the lowest point is a Fokker-Planck calculation in which the residual dc electric field was arbitrarily set to zero. This lowest point should be compared with the field-free TORAY calculations. The analyses span a factor of two in inferred current drive efficiency. Although the agreement between the Fokker Planck for $E_{\rm dc} = 0$ and TORAY for the experimentally measured $n_{13}(0) = 1.2$ and $T_e(0) = 2.5$ keV is not extremely good, the experimental and calculational uncertainties are fairly large and could be accounted for by uncertainties in the kinetic profiles, for example. The ECE spectrum calculated by

the Fokker-Planck code is in good agreement with the experimental measurements. Figure 3 summarizes the TORAY output, showing ray tracing, power deposition, and the ECE data from CQL3D.

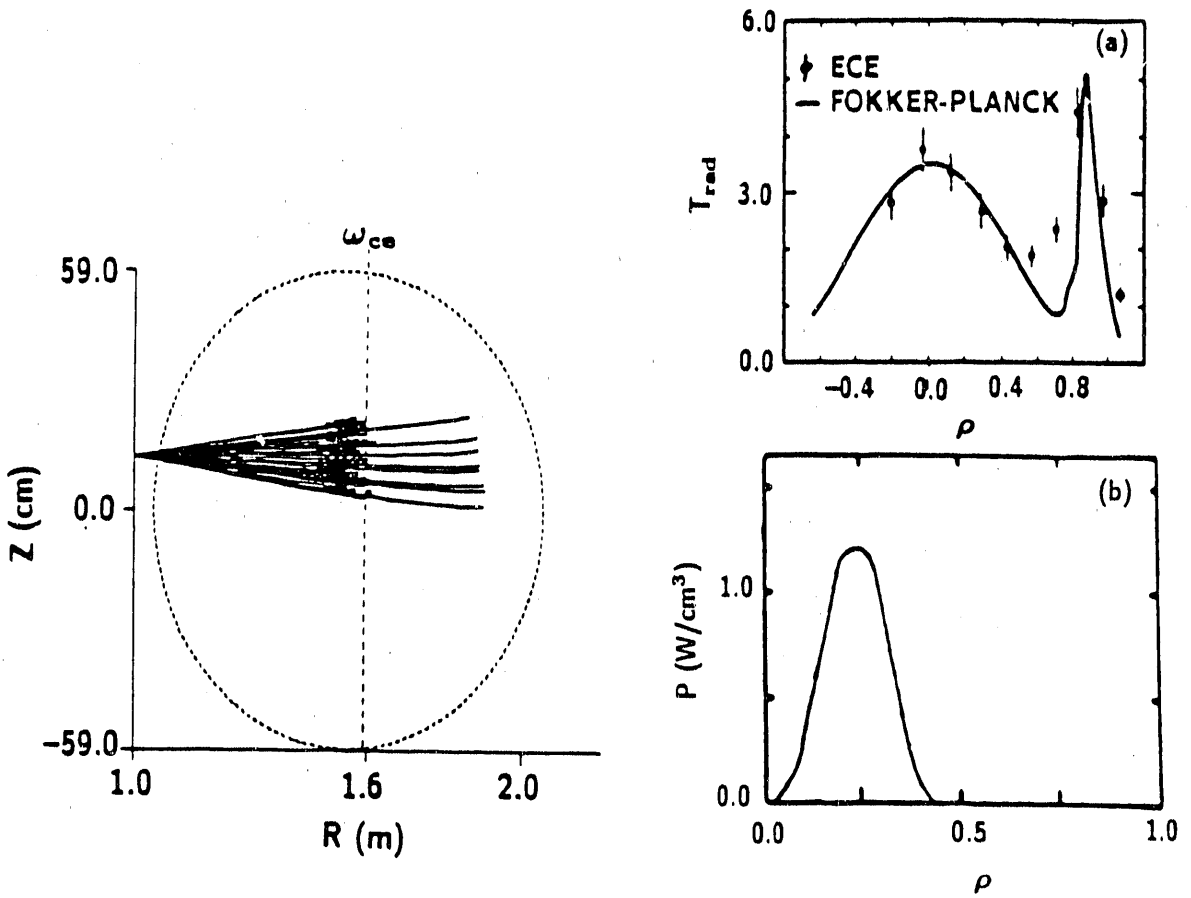

Fig. 3. TORAY output and the ECE spectrum calculated by CQL3D for the DIII–D experiment. The resonance was at the magnetic axis and $\bar{n}_e \sim 1.2 \times 10^{13}$ cm^{-3}.

The non-linear interaction between electrons accelerated into the superthermal tail and the residual field was considered by Giruzzi, who found in an independent Fokker-Planck calculation that such a residual dc electric field could increase the current which appeared to be rf-driven by as much as a factor of two. These results are summarized in Fig. 4. Here the ratio of the current observed with no dc electric field to that with electric field is plotted as a function of the electric field normalized to the critical (Dreicer) field. Considering the T_e dependence of the critical field, both 2 and 4 keV temperatures give the same enhancement. The additional current can be equal to the rf-driven current, and when the DIII–D measurement is

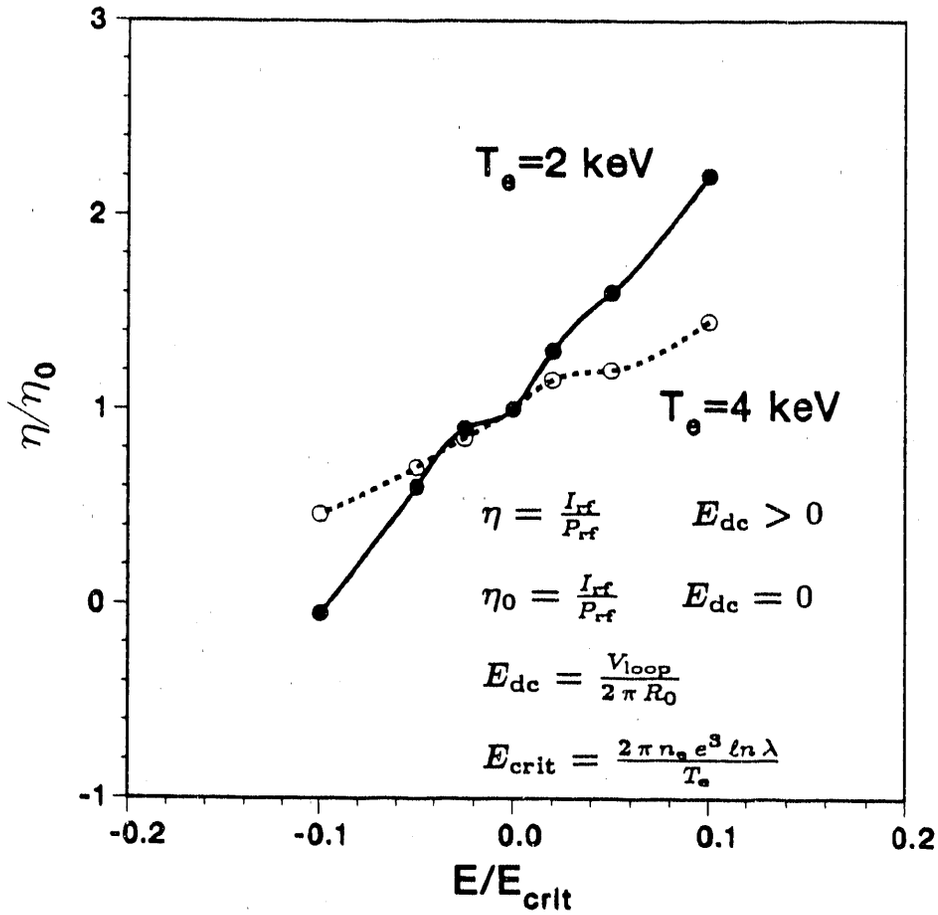

Fig. 4. The effect of a residual dc electric field is shown by the enhanced current in the co-direction as a function of the electric field normalized to the critical (Dreicer) field for electron run-away. The factor of two enhancement at fields present in the experiment is consistent with the loop voltage measurement for co versus counter rf current generation and with the correction required to obtain agreement between the measurement and field-free TORAY.

corrected for this phenomenon, the rf-driven current at $E_{dc} = 0$ is recovered for comparison with TORAY.

To address this issue experimentally, the direction of the inductive current, and therefore the dc electric field, was reversed and the current drive experiment was repeated with the rf-driven current opposing the inductive current. In this case the measured loop voltage was greater than that calculated from the profiles, indicating an rf-driven component opposing the inductive current. Approximately a factor of two difference between the co- and counter-rf current cases was found, suggesting that this analysis is qualitatively correct. TORAY calculations agree with the corrected experimental data.

B. T–10 Low Field O–Mode Current Drive

The relatively good agreement between theory and experiment in the DIII–D case suggests that the T–10 experiment can be described reasonably well by TORAY and CQL3D. A series of calculations was performed with TORAY in which the density, temperature, and resonance radius were varied for the T–10 geometry as described above. The results are shown in Fig. 5.

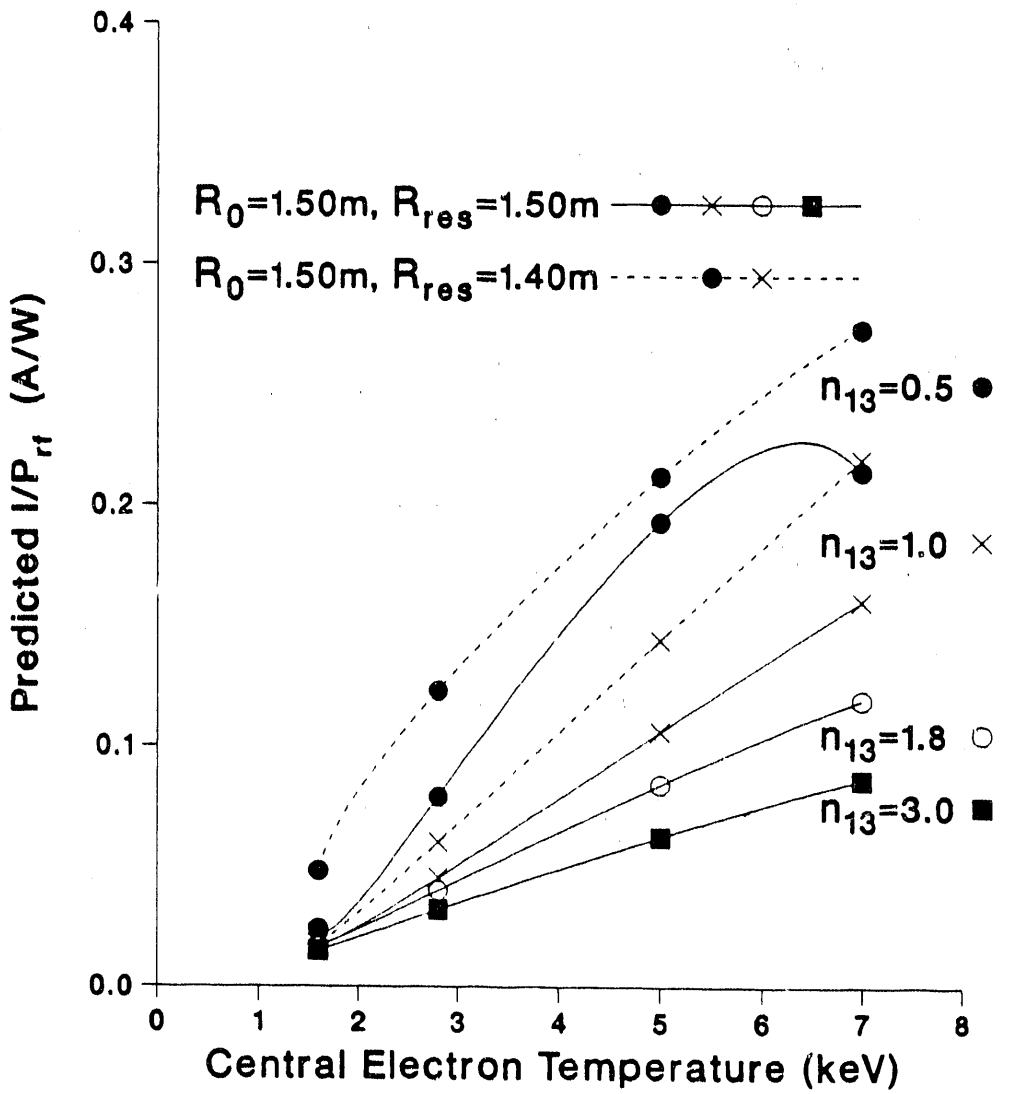

Fig. 5. TORAY calculations of the current drive expected for T–10 from the "Sector B" geometry shown in Fig. 1. Highest current drive requires low density, high temperature and a resonance at $R \sim 140$ cm. From these calculations, T–10 could achieve rf driven currents greater than 400 kA.

Calculations were performed for four values of central electron temperature and four values of central density. The *ad hoc* profiles were approximately

$$T_e(r) = T_e(0)(1 - r^2/a^2)^{1.5} \quad ,$$

and

$$n_e(r) = n_e(0)(1 - r^2/a^2)^{0.5} \quad .$$

For most of the calculations the ECH resonance was placed at the geometric center of the machine, but for central densities of $1.0 \times 10^{13}/\text{cm}^3$ and $0.5 \times 10^{13}/\text{cm}^3$ the resonance was also located at $r = -10$ cm.

In general, current drive efficiency increases approximately linearly with electron temperature and decreases linearly with density. There is a very large increase in current drive efficiency when the density is reduced below $1 \times 10^{13}/\text{cm}^3$.

For achievable values of T_e and n_e on T–10, efficiencies as high as 0.10 → 0.20 A/W should be realized. This is approximately three times the efficiency measured in the DIII–D experiment owing primarily to better localization of the absorption at the hottest region of the discharge with low field launch. Because of the relativistic mass shift of the superthermal population the resonance should be located inside the magnetic axis so that resonant damping will actually occur near the center of the discharge where T_e is highest. This also reduces trapped particle effects. At a central density of $1 \times 10^{13}/\text{cm}^3$ the efficiency is approximately 40% greater with the resonance at $r = -10$ cm compared with the resonance at $r = 0$.

The Fokker-Planck code CQL3D was exercised for a hypothetical DIII–D experiment employing low field launch of the O–mode and the current drive efficiency as a function of launch angle was calculated. Although done for DIII–D, the calculation is for circular cross section and is generally applicable to T–10. The results, plotted in Fig. 6 along with TORAY calculations for the same cases show a broad maximum in efficiency for launch angles between 15 degrees and 25 degrees from perpendicular.

The Fokker-Planck calculations agree fairly well with the ray tracing at low power, however exhibit up to a factor of two enhancement in efficiency over the TORAY estimate at higher power. This enhancement over the linear regime efficiency is due to a quasi-linear increase

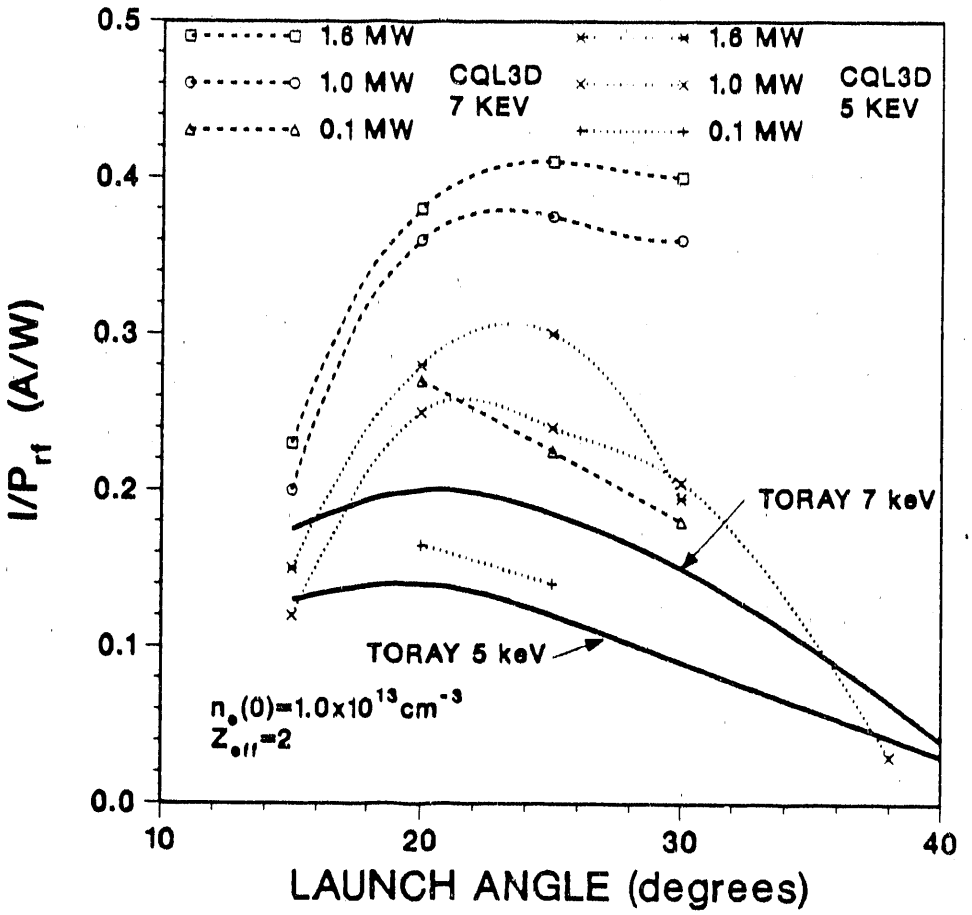

Fig. 6. Fokker-Planck and TORAY calculations for 60 GHz low field launch O–mode fundamental heating on DIII–D showing a substantial enhancement in current drive at high power. These results are relevant for the T–10 experiment as well.

in the tail electron population and to a decrease in the trapping of heated electrons owing to relativistic effects. Neither of these phenomena is modeled by TORAY. The result is encouraging for the T–10 experiment because of the very large rf powers, possibly greater than 3 MW, which could be available.

The distribution function of Eq. (1) was used in TORAY to model the effect of a superthermal tail on the spatial distribution of both the absorption and driven current. The results are plotted in Fig. 7 for the parameters listed in Table I.

It is seen that the superthermal tail leads to a substantial increase in the current drive efficiency over that for the Maxwellian. The calculations also illustrate the excellent localization of the driven current, which may mean that current generation, for example, in the vicinity of the $q = 2$ surface could be employed to stabilize tearing modes and prevent disruptions.

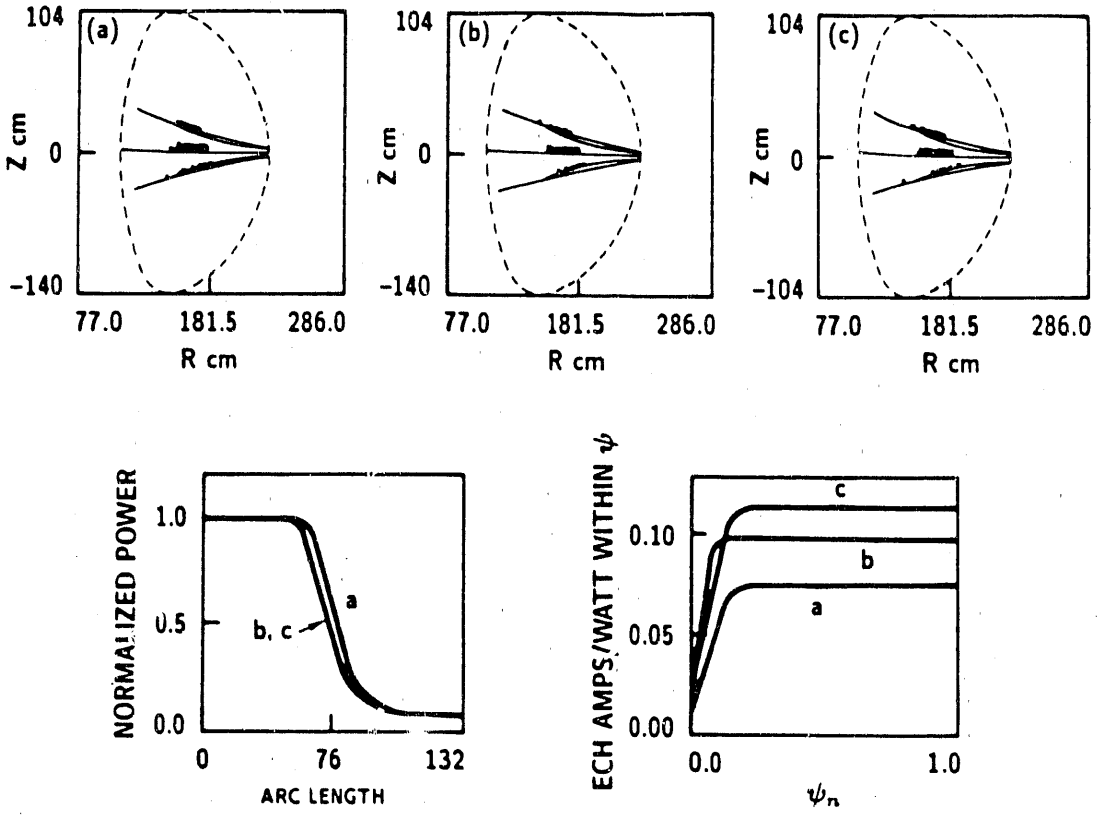

Fig. 7. With the addition of a suprathermal tail, TORAY predicts a substantial increase in current drive efficiency compared with a Maxwellian.

TABLE I

Curves	Tail Density (%)	$T_e(0)$ (keV)	$T_{\parallel f}$ (keV)	$T_{\parallel b}$ (keV)	$T_\perp$ (keV)	ρ
a	0	5	–	–	–	
b	5	5	15	7	10	0
	5		5	3	5	1
c	5	5	20	10	13	0
	5		7	5	6	1

Additional work must be done to examine the deleterious effects of trapping and possibly unstable $j(r)$ profiles.

V. FUTURE PLANS FOR DIII–D

On the DIII–D tokamak, installation of a low field spatially scannable launcher system for 110 GHz has begun. The present plan calls for operation of a four 500 kW gyrotrons capable of 10 second pulses in late 1991 in addition to the existing 2 MW, 60 GHz system. The

waveguide transmission line will propagate the HE_{11} mode and be evacuated, thus eliminating the machine vacuum window. The transmission system [8] is shown schematically in Fig. 8, and a photograph of the first steerable launcher assembly currently installed on DIII–D is shown in Fig. 9. The launched waves will be X–mode at 20 degrees to the radial.

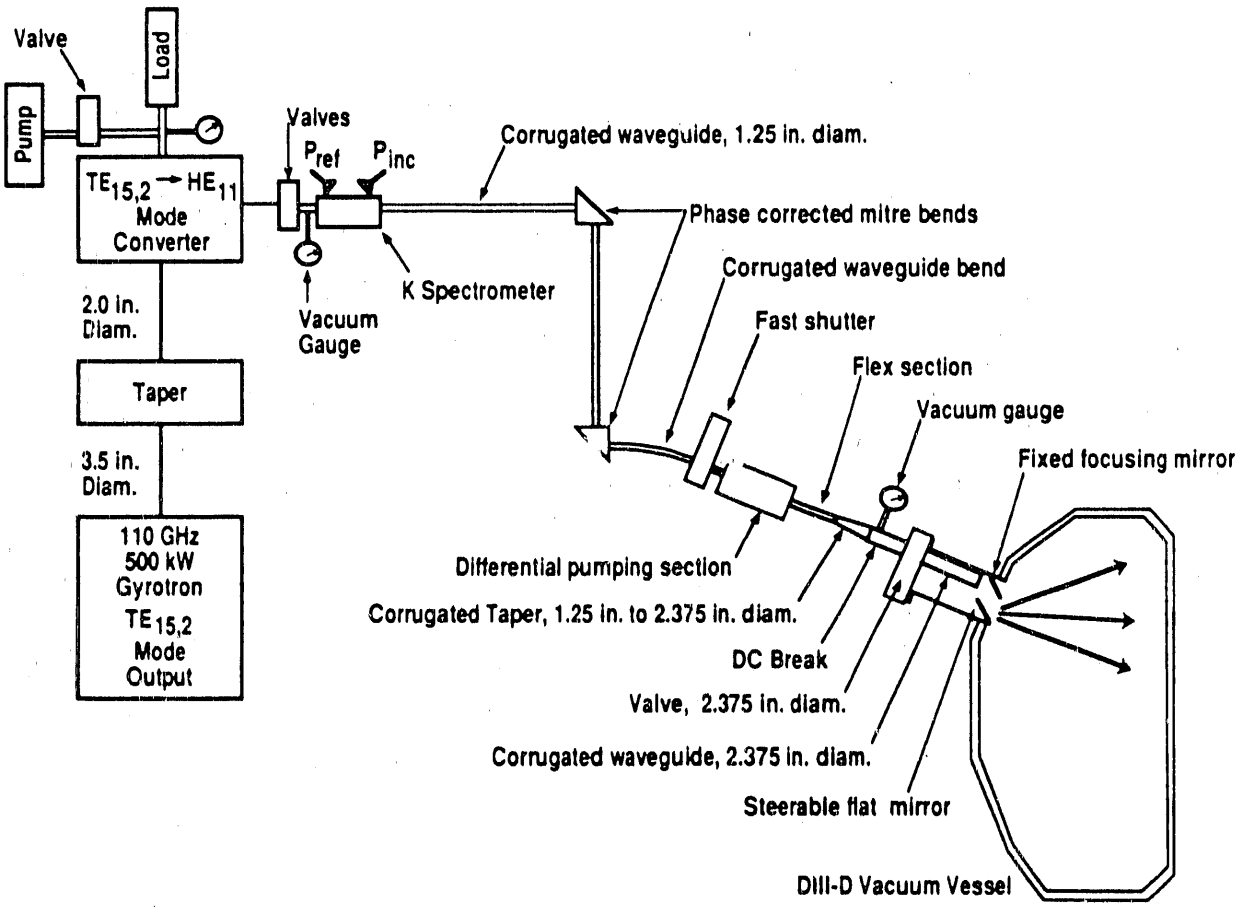

Fig. 8. Schematic of the evacuated 110 GHz transmission line for DIII–D. The rf power can be scanned across the plasma by moving a mirror.

Preliminary TORAY calculations for second harmonic X–mode low field launch, done for the parameters of Table I, show that the current drive efficiency may be ~30% greater than the low field O–mode fundamental efficiency and that the efficiency is only weakly dependent on the presence of a superthermal tail. These calculations are summarized in Fig. 10.

VI. CONCLUSIONS

Model calculations have been performed for both the DIII–D and T–10 electron cyclotron current drive experiments. Agreement between the calculations and measured non-inductive current on DIII–D is good, increasing the confidence in the predictions of 0.1–0.2 amperes/watt

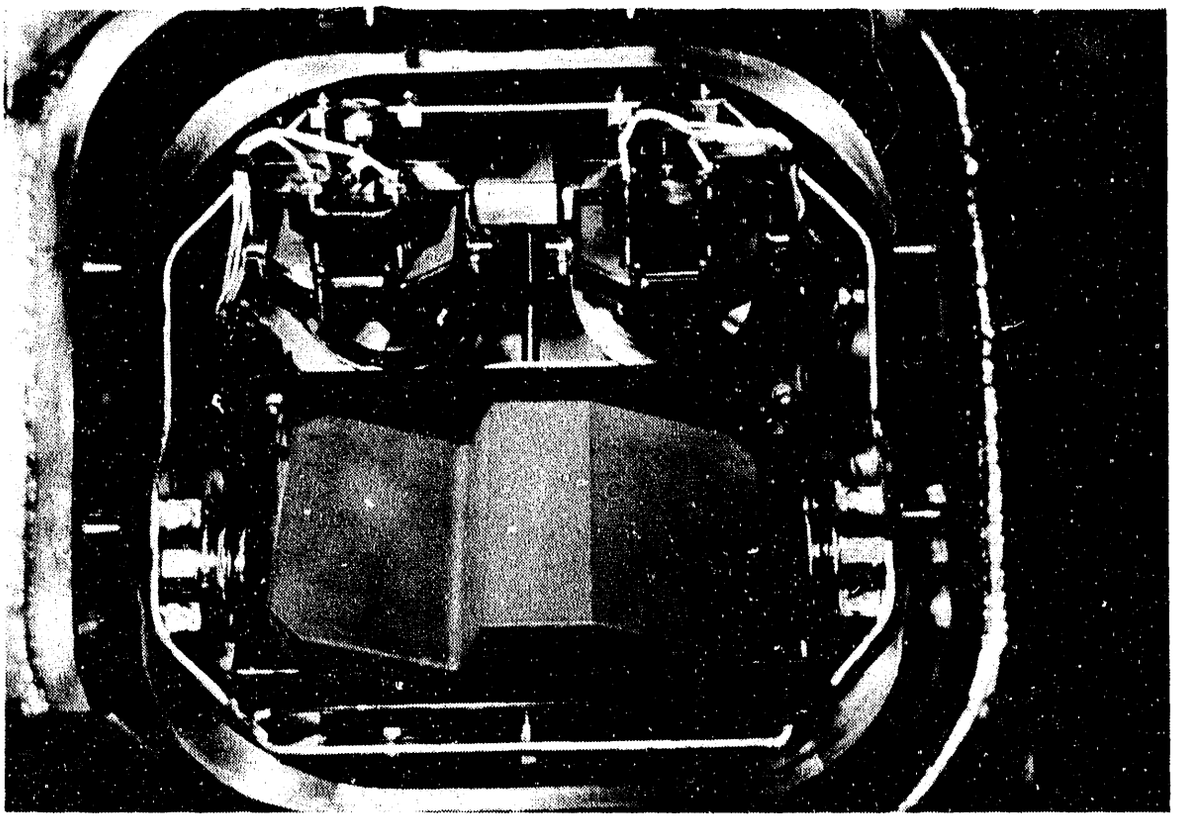

Fig. 9. Photograph of the first steerable launcher installed on DIII–D. This assembly accommodates two rf beams and injects into the torus at an angle of approximately 20 degrees to the radial for current drive experiments. The assembly is approximately 30 cm across.

for T–10. Fokker-Planck calculations indicate that non-linear effects at high power may further enhance the current drive efficiency on T–10. The location of the ECH resonance should be inside the magnetic axis to realize the best efficiency. Installation of the DIII–D 110 GHz system has begun.

REFERENCES

[1] Lloyd, B., Edlington, T., O'Brien, M.R., *et al.*, Nucl. Fusion **28**, (1988) 1013.

[2] Moeller, C.P., Prater, R., Riviere, A.C., *et al.*, Proceedings of 6th Joint Workshop on Electron Cyclotron Emission and Electron Cyclotron Resonance Heating. Oxford (1987), Culham Report CLM-ECR, 355 (1987).

[3] Matsuda, Kyoko, IEEE Transactions on Plasma Science **17**, (1989) 6; Kritz, A.H., Hsuan, H., Goldfinger, R.C., and Batchelor, D.B., in Proceedings of 3rd Joint Varenna-Grenoble International Symposium on Heating in Toroidal Plasmas, Brussels, (1982) Vol. 2, p. 707.

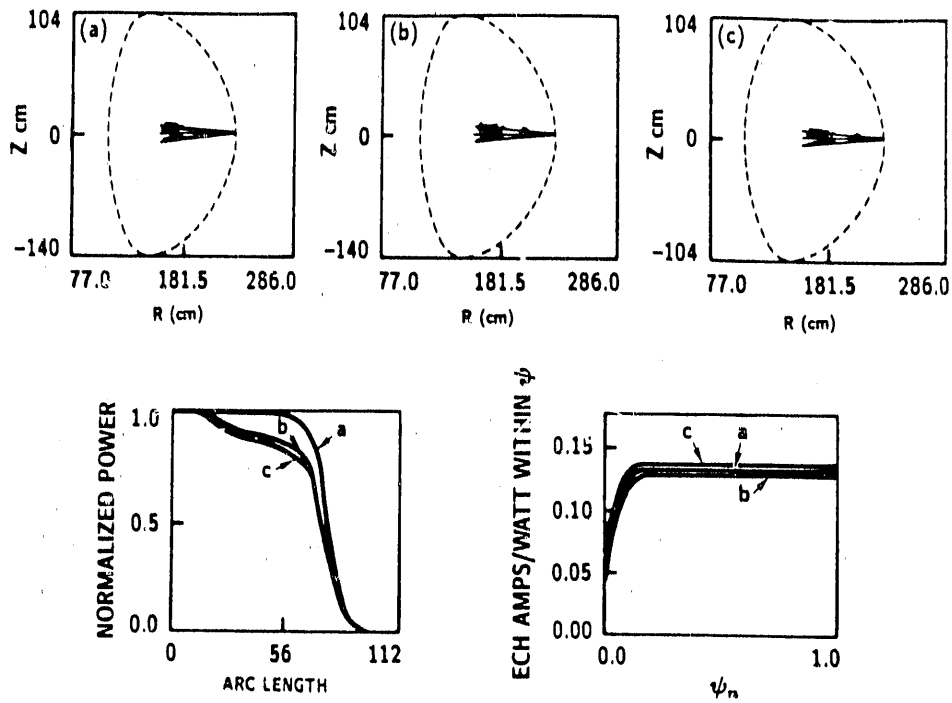

Fig. 10. Preliminary TORAY calculations for the DIII–D 110 GHz low field launch second harmonic X–mode experiment. Damping is excellent and is not extremely sensitive to the presence of a suprathermal distribution function.

[4] Cohen, R.H., Phys. Fluids **30**, (1987) 2442.

[5] Pfeiffer, W.W., Davidson, R.H., Miller, R.L., and Waltz, R.E., General Atomics report GA–A16178 (1980).

[6] Harvey, R.W., McCoy, M.G., and Kerbel, G.D., in Applications of Radio Frequency Power to Plasmas, American Institute of Physics Conference Proceedings **159**, Kissimmee, (1987) p. 49.

[7] Giruzzi, G., this conference.

[8] Moeller, C.P., Prater, R., Callis, R.W., *et al.*, Proceedings of the 16th Symposium on Fusion Technology, London (1990).

END

DATE FILMED

01 / 11 / 91